Computational Materials Science 213 (2022) 111619

Contents lists available at ScienceDirect

Computational Materials Science

journal homepage: www.elsevier.com/locate/commatsci

Examining the thermodynamic stability of mixed principal element oxides in AlCoCrFeNi high-entropy alloy by first-principles

Indranil Roy [a], Chinedu Ekuma [b,c], Ganesh Balasubramanian [a,c,*]

[a] Department of Mechanical Engineering & Mechanics, Lehigh University, Bethlehem, PA
[b] Department of Physics, Lehigh University, Bethlehem, PA
[c] Institute for Functional Materials and Devices, Lehigh University, Bethlehem, PA

ARTICLE INFO

Keywords:
High-entropy alloy
Density functional theory
Oxidation
Thermodynamic stability
Formation energy

ABSTRACT

Understanding the complex oxidation behavior of alloys consisting of multiple principal elements is critical to realize their potential for high temperature structural applications. We examine the thermodynamic stability of primary and mixed oxides for one such extensively examined high-entropy alloy (HEA), AlCoCrFeNi, using first-principles calculations. Our predictions indicate that Cr_2O_3 and Al_2O_3 are the most stable oxides both at the ground state and elevated temperatures, with the relative ordering for oxide stability at higher temperatures being similar to that at 0 K. The presence of both Al with Cr are most likely to form protective oxide layers, while that produced by Ni and Cr are the least stable. Nevertheless, the gradient of formation energies for the stable mixed Cr_2O_3-type oxides with increasing concentration of other principal elements becomes steeper with increasing temperature.

Since the first report on high-entropy alloy (HEA) in 2004 [1], extensive studies have been performed on different classes (*e.g.,* refractories and those composed of transitional metals) of HEAs, which are near equimolar concentrated solid solutions of five or more elements. These intriguing materials have garnered significant interest due to their potential for notable structural properties at high temperatures [2], which situates them as a possible cost-efficient alternative for Ni-based superalloys. Nevertheless, elevated temperature applications such as in gas turbine blades, require a thorough understanding of high-temperature oxidation and an alloy design to mitigate the risks. The complexity of HEA oxidation emerges from the various simple and mixed oxide chemistries that can form due to the presence of multiple principal elements. A systematic computational approach can enable a fundamental physics-based understanding of the complex oxidation mechanisms, to supplement and streamline the experimental scrutiny and material design. The first step towards such modeling is to identify the stable oxides for a given composition of the alloy. In the case of the widely-reported AlCoCrFeNi [3–5] HEA, the presence of Cr and Al in the alloy contributes to the formation of protective chromia (chromium (III) oxide) and alumina (aluminum (III) oxide) scales on the surface, preventing uninhibited oxidation of the HEA [6].

Sparse experimental [6–11] and computational [12,13] studies on AlCoCrFeNi oxidation exist, but a fundamental understanding of the thermodynamic stability of simple and mixed oxides that form in this HEA is limited. Butler *et al.* [6] studied the effect of varying Al content in $Al_x(NiCoCrFe)_{100-x}$ (where x = 8, 10, 12, 15, 20, and 30 at.%) during oxidation at 1050 °*C* for 50 h, and found a continuous external chromia (Cr_2O_3) scale at all concentrations of Al. The alumina (Al_2O_3) formed discontinuously at low Al concentration (x = 8,10,12) while a thick Al_2O_3 layer was reported for higher fractions of Al (x = 15, 20, and 30 at. %) in the HEA, corroborating that an increase in Al content improves the oxidation resistance. Oxidation of AlCoCrFeNi (with 1.24 at. % Al) in the temperature range of 800 °*C* to 1000 °*C* was compared against the commercially available 825 Ni-based alloys and the duplex 2205 stainless steel (DSS) [7]. Experiments showed that at 1000 °*C*, the HEA had the least mass gain, while the DSS (that has a high concentration of Fe) gained the highest mass; for the HEA and the Ni-based alloy with 25 at. % and 30 at. % Fe content, respectively, mass gain recedes after 60–70 hours. In absence of Al, the protective oxide layer for the commercial alloys primarily contain chromia and Fe-oxides. Al assists in the formation of a protective thin chromia layer on the HEA surface, while alumina containing internal oxidation zones were found in the bulk material[9]. The local atomic environment of oxygen on the surface [12,14] and in the interstitial sites [13,15] were reported to be

* Corresponding author at: Packard Laboratory 561, 19 Memorial Drive West, Bethlehem, PA 18015, USA.
E-mail address: bganesh@lehigh.edu (G. Balasubramanian).

https://doi.org/10.1016/j.commatsci.2022.111619
Received 17 April 2022; Received in revised form 20 June 2022; Accepted 22 June 2022
Available online 28 June 2022

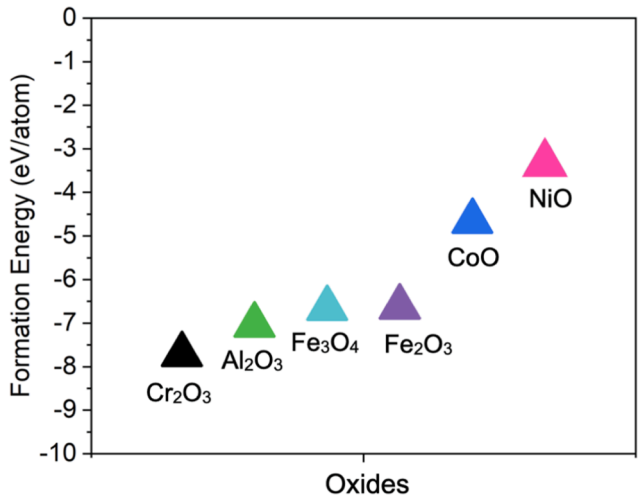

Fig. 1. The formation energies of single element primary oxides of Al, Co, Cr, Fe, and Ni that constitute the HEA, as computed at the ground state (0 K).

important for preferential oxidation; Liu *et al.* [13] concluded that oxygen in an interstitial site is more stable near a Cr atom than a Ni atom.

Here, we examine the thermodynamic stability of simple and mixed oxides that can form during the oxidation of AlCoCrFeNi using *ab initio* computations. Complementing the previous studies where the HEAs incorporate oxygen on the surface and in the interstitial sites, our independent treatment of the bulk oxides contributes to understanding the oxidation mechanisms in various complex alloys composed of Al-Co-Cr-Fe-Ni elements.

The first-principles calculations are performed with Vienna Ab initio Simulation Package (VASP) [16,17]. The oxide structures are obtained from the Materials Project database[18]. The generalized gradient approximation (GGA) as parameterized by Perdew–Burke–Ernzerhof (PBE) is chosen as the exchange–correlation functional [19,20]. A $5 \times 5 \times 5$ k-point grid with the Monkhorst–Pack method [21] is used to sample the reciprocal space with a cutoff energy of 500 eV, which ensured the energy (charge) is converged to within 10^{-7} eV (10^{-3} eV), with the residual stresses and forces less than 0.02 GPa and 10^{-3} eV/Å, respectively.

Before the energetic calculations, the ions and forces of the system are first relaxed, and self-consistency calculations are performed on the relaxed structures. The formation energy of $A_xB_yO_z$ oxide is obtained from $E_{A_xB_yO_z} = G_{A_xB_yO_z} - xG_A - yG_B - zG_O$, where G_{AxByOz} is the Gibbs free energy of oxide, while G_i is the Gibbs free energy of one i atom placed at the center of the simulation cell [22]. The total energy for the oxide and the individual atoms are used to compute the Gibbs free energy in the above equation. The mixed oxides are constructed using the special quasi-random structures (SQS) method within the mcsqs utility in the Alloy Theoretic Automated Toolkit (ATAT) that can generate random solid solutions [23] with varying concentrations of foreign elements. We note that the initial structure of both Cr_2O_3 and Al_2O_3 consists of 10 atoms in a trigonal unit cell. Among the 4 cations in the 10-atom unit cell, 1, 2, and 3 cations are respectively altered from parent cation to foreign cation to create mixed oxides with 25%, 50%, and 75% of foreign element addition. The supercell size is carefully chosen to contain the minimum number of atoms per unit cell. We perform selective simulations on larger supercells to verify and eliminate any role of size effect on the results. We add foreign metals to the oxides for mixed oxide formation by fractionally replacing the base metal with the foreign element. The size of the supercell was chosen accordingly to accommodate a minimum number of atoms required for creating the composition of the mixed oxide. For example, a unit cell with 10 atoms is sufficient to accommodate 25%, 50%, and 75% of foreign cations. So, a supercell of $1 \times 1 \times 1$ is used for SQS. As we need a minimum of 4 parent cations to create mixed oxides, the supercell size is different for each simulated case.

For the *ab initio* molecular dynamics (AIMD) simulations, a larger supercell is constructed with at least 120 atoms by relaxing the forces and stresses of the unit cell, and replicating the SQS-derived structure in all three directions. An additional increase in the number of atoms essentially raises the computational cost with negligible change in the results. The system is equilibrated constraining the number of atoms (N), volume (V), and temperature (T) under the canonical (NVT) ensemble using the Nose-Hoover thermostat with a coupling time of 5 picoseconds. These simulations are initially run for 5000 steps with 1 picosecond timestep, but the energy typically converges after 2000 steps.

Thermodynamic stability of primary oxides: The oxides of each element in AlCoCrFeNi can have multiple oxidizing states depending on the variable oxidation number and a given oxide may have more than one stable phase. For instance, Cr has oxidation numbers of + 3, +2, and + 1 [24], and Cr_2O_3 has two phases, viz., trigonal and cubic, though only the former is stable. Likewise, the oxides of Al, Co, Fe, and Ni have multiple stable oxidizing states. Since the common oxidation states of all the elements of this HEA are well reported, we calculate the ground state formation energies to interrogate the relative thermodynamic stabilities of the various oxides (Fig. 1). The formation energies are computed per molecule of the oxide. For consistency, Fig. 1 displays energies per atom of the oxides. The lower the formation energy, *i.e.*, the more negative the magnitude, the more stable is the material. The negative sign is a result of the formation energy calculation from the Gibbs free energies of the various constituents of the system. Hong et al. [12] found the cohesive energy of chromia to be slightly higher than alumina due to the low Pauling electronegativity and valance electron count of Al_2O_3. We find that Cr_2O_3 has the lowest formation energy followed by Al_2O_3 amongst all the oxides that can form in AlCoCrFeNi HEA, in accord with earlier experimental reports that suggest the formation of Cr_2O_3 and Al_2O_3 as the primary oxide layers for this alloy [6,7,25]. While our results, in agreement with certain prior reports but in contrast to Ellingham diagrams (at higher temperatures), indicate that Cr_2O_3 is more stable than Al_2O_3 in the ground state, we do note that above 1250 K, Cr_2O_3 is volatile and dissociates, rendering Al_2O_3, as the most stable oxide that forms a passivating layer. We plan to perform additional calculations in the future on the mechanical stability of these oxides at the ground state and at higher temperatures to address this issue. The relatively high formation energies for NiO and CoO impede their occurrence in this HEA [26]. Note that certain oxides of reactive elements (REs), such as HfO_2, assume lower formation energy than Cr_2O_3 and form very stable oxides quickly, but are not often used due to the high cost associated with REs [9].

The results from our AIMD simulations for the thermodynamic stability of the oxides at 1000, 1250, and 1500 K, are presented in Table 1.

Table 1
The formation energy per atom (eV/atom) of single element primary oxides of Al, Co, Cr, Fe, and Ni that constitute the HEA, computed at ground state (0 K) and at elevated temperatures (1000 K, 1250 K, and 1500 K).

Temperature	Cr_2O_3	Al_2O_3	Fe_3O_4	Fe_2O_3	CoO	NiO
0 K	−7.7187	−7.0415	−6.6605	−6.6296	−4.663	−3.3271
1000 K	−7.2185	−6.3539	−6.0493	−6.0819	−4.4088	−2.6247
1250 K	−7.1845	−6.3284	−6.0129	−6.0426	−4.3526	−2.5652
1500 K	−7.1502	−6.2959	−5.9562	−6.011	−4.2984	−2.5147

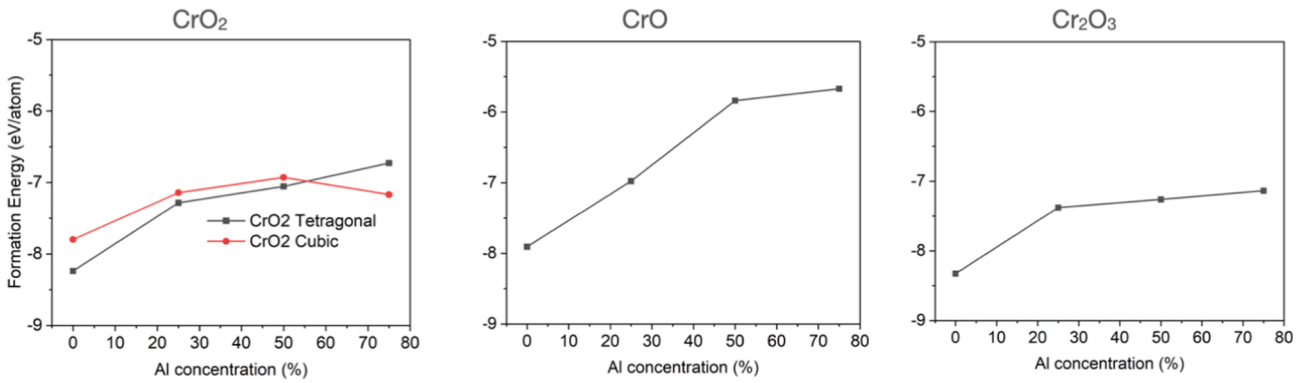

Fig. 2. The formation energies of (a) CrO_2, (b) CrO and (c) Cr_2O_3 at the ground state computed for varying concentrations of Al present in the oxide.

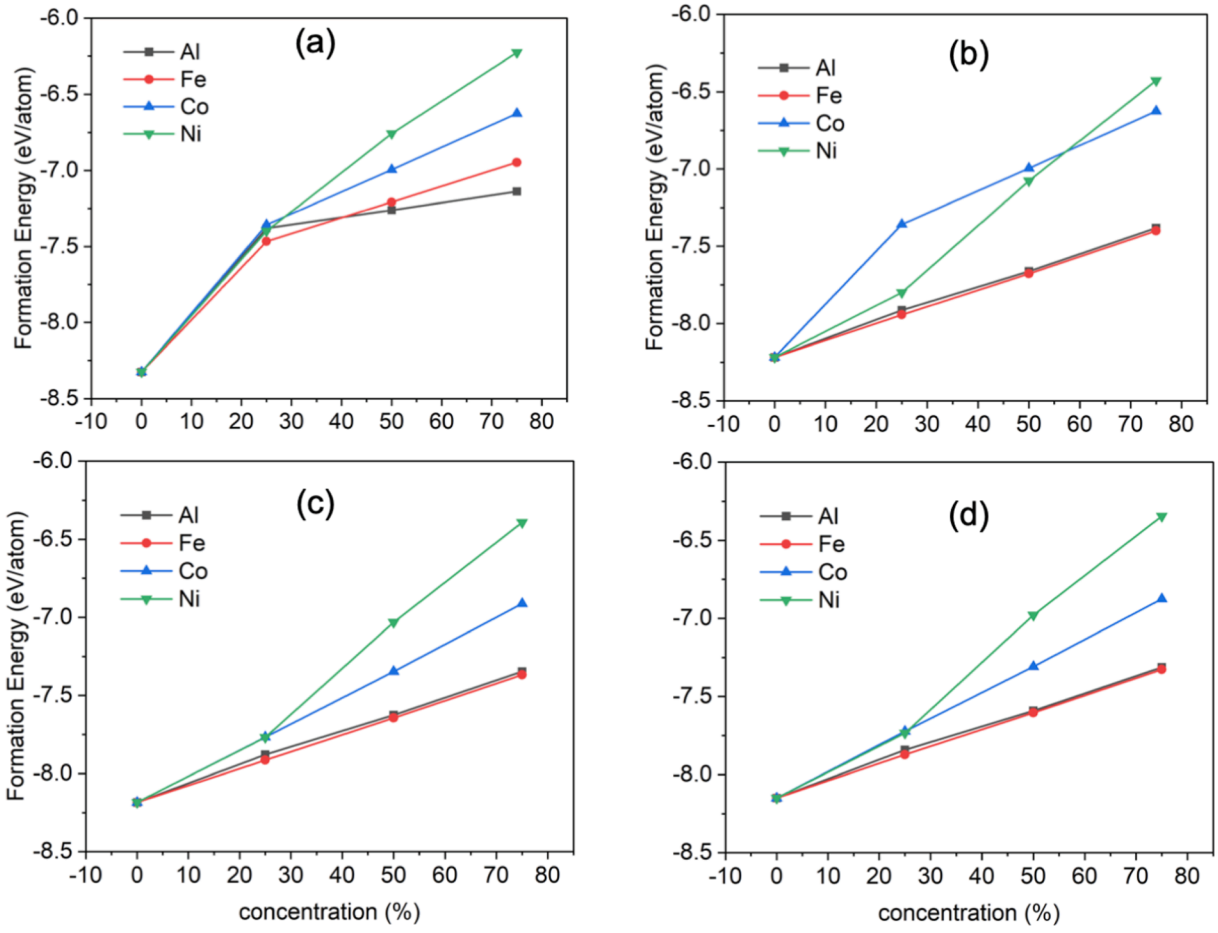

Fig. 3. The formation energies of mixed Cr_2O_3-type oxides at (a) ground state, (b) 1000 K, (c) 1250 K, and (d) 1500 K. The mixed oxides with 25%, 50%, and 75% concentration of the other principal element assume the chemical formula of XCr_3O_6, $XCrO_3$, and X_3CrO_6, respectively, where X = Al, Co, Fe, and Ni. The mixed oxides considered here are solid solution oxide of Cr and X, where the latter as the foreign element has replaced the base metal. For instance, XCr_3O_6 indicates that there is one X metal atom in a supercell of Cr_4O_6 oxide, forming XCr_3O_6. We have not used the convention of brackets to avoid confusion of how many atoms are present in one mixed oxide molecule. An alternate representation is $X_yCr_{(1-y)}O_3$ where y = 0.25, 0.5 and 0.75.

While the energies demonstrate a trend similar to the ground state, a quantitative assessment indicates that formation energies increase with temperature for all the oxides. At elevated temperatures, Cr_2O_3 is the most and NiO is the least stable. Nevertheless, given the volatile nature of Cr_2O_3 above 1250 K when it is known to dissociate [27], the next most stable oxide is Al_2O_3, which also forms a passivating layer, and is critical for high-temperature oxidation resistance of AlCoCrFeNi high entropy alloy.

Thermodynamic stability of Cr-oxides: Zhu *et al.* [7] suggested that the presence of Cr in the oxide scale enables AlCoCrFeNi to be a strong oxidation-resistant alloy. Although Cr_2O_3 is the primary oxide, other Cr oxides may form. Since Al concentration exerts a significant influence on the oxidation resistance of AlCoCrFeNi, we scrutinize the formation energies of all possible Cr and Al mixed oxides with varying Al concentrations. For 25%, 50%, and 75% Al addition in Cr_2O_3, the mixed oxide chemistries are $AlCr_3O_6$, $AlCrO_3$, and Al_3CrO_6, respectively. Additionally, we consider two phases of CrO_2, tetragonal and cubic, and CrO for the calculations. In the absence of Al, Cr_2O_3 has the lowest

formation energy (-42 eV), followed by CrO_2 (-24.8 eV for cubic and –23.2 eV for tetragonal) and CrO (-16.1 eV). With the increase in Al content, the formation energies of all the Cr-oxides increase, as shown in Fig. 2. Mixed oxides with high fractions of Al in CrO are least stable, while Cr_2O_3 is most stable even in presence of Al and is anticipated to form a passivating layer.

Thermodynamic stability of mixed oxides: The other principal elements (Co, Fe, and Ni) in the HEA can also form a mixed oxide with Cr_2O_3. As discussed above, NiO and CoO are the least stable primary oxides. When Ni is mixed with Cr_2O_3, the increase in the formation energy is almost linear, as shown in Fig. 3a. Thus, the Ni-Cr mixed oxides are unstable, especially at high Ni concentrations. Co addition has a similar effect on Cr_2O_3, though the oxides with high Co content have enhanced thermodynamic stability than high Ni-containing ones. Mixed oxides of Fe and Cr exhibit low formation energies, producing relatively stable oxides. An earlier experimental report on the oxidation behavior of AlCrCoFeNi, 825 Ni-based alloys, and 2205 duplex stainless steel (DSS) revealed that 2205 DSS was the poorest among the three alloys with the scale containing considerable Fe-oxide. Results from our simulations corroborate that, unlike Cr_2O_3 and Al_2O_3, Fe_3O_4 is not a passivating oxide scale. It implies that a HEA with Cr but devoid of Al will have poor oxidation resistance, especially at high temperature, with the oxide layer predominantly composed of Fe_3O_4. Although the formation energy scarcely changes with an increasing Al content in Cr_2O_3, we find that the addition of 25% of other principal elements in Cr_2O_3, *e.g.*, to form XCr_3O_6 (where X = Al, Co, Fe, Ni), assumes near-equal formation energies. The differences in oxide stabilities are more notable when a higher fraction of the principal elements form mixed oxides.

At elevated temperatures, the energies of mixed oxides in Cr_2O_3 are reproduced in Fig. 3(b-d). The temperatures presented in Fig. 3 are chosen to examine the high-temperature response of these oxides as applicable to potential aerospace and power generation industries. While the exact values of the temperatures do not offer direct quantitative guidance, but the trends provide qualitative insight on the oxide stabilities. Similar to 0 K results, Al and Fe form low energy stable oxides with Cr while a high concentration of Ni renders Cr_2O_3 unstable. Cr_2O_3 forms comparably stable mixed oxides with both Al and Fe for significantly high proportions of the principal elements, even at elevated temperatures. Interestingly, the rate of increase of formation energy with increasing concentration of principal elements displays a constant gradient, in contrast to the saturating profile noted from ground state calculations. The results assert that in the presence of other principal elements, Cr_2O_3 becomes less stable at a faster rate at higher temperatures than in the ground state.

In summary, we have examined the thermodynamic stability of primary and mixed oxides in AlCoCrFeNi high-entropy alloy from first-principles and *ab initio* molecular simulations. From the predictions for the formation energies, we corroborate that Cr and Al form the most stable oxides, *i.e.,* chromia and alumina, in agreement with experimental literature. Given the presence of multiple principal elements, we find that mixed oxides of chromia are stable even when containing high percentages of Al. At elevated temperatures, the mixed oxides exhibit a similar trend for relative stabilities as in their ground states, although the increase in formation energies with increasing concentration of principal elements is steeper than that at 0 K. Further efforts, including examining the thermodynamic stability of spinels that can affect the oxidation pathways in multicomponent alloys, are required to elucidate the fundamentals of the complex oxidation mechanisms in HEAs. This assessment of the preferential oxide formation in a model HEA provides guidelines for designing oxidation-resistant multicomponent alloys.

CRediT authorship contribution statement

Indranil Roy: Data curation, Formal analysis, Investigation, Methodology, Visualization. **Chinedu Ekuma:** Formal analysis, Methodology. **Ganesh Balasubramanian:** Conceptualization, Investigation, Funding acquisition, Project administration.

Declaration of Competing Interest

The authors declare that they have no known competing financial interests or personal relationships that could have appeared to influence the work reported in this paper.

Acknowledgement

The research was supported by the National Science Foundation (NSF), United States through the awards CMMI-1944040, OAC-2019035, and DMR-2202101. Any opinions, findings, conclusions, or recommendations expressed in this material are those of the authors and do not necessarily reflect the views of the NSF.

Data Availability

Data will be made available upon reasonable request.

References

[1] J.-W. Yeh, S.-K. Chen, S.-J. Lin, J.-Y. Gan, T.-S. Chin, T.-T. Shun, C.-H. Tsau, S.-Y. Chang, Nanostructured High-Entropy Alloys with Multiple Principal Elements: novel Alloy Design Concepts and Outcomes, Adv. Eng. Mater. 6 (5) (2004) 299–303, https://doi.org/10.1002/adem.200300567.
[2] C.-Y. Hsu, C.-C. Juan, W.-R. Wang, T.-S. Sheu, J.-W. Yeh, S.-K. Chen, On the superior hot hardness and softening resistance of AlCoCrxFeMo0.5Ni high-entropy alloys, Mater. Sci. Eng. A. 528 (10-11) (2011) 3581–3588, https://doi.org/10.1016/j.msea.2011.01.072.
[3] Z. Tang, O.N. Senkov, C.M. Parish, C. Zhang, F. Zhang, L.J. Santodonato, G. Wang, G. Zhao, F. Yang, P.K. Liaw, Tensile ductility of an AlCoCrFeNi multi-phase high-entropy alloy through hot isostatic pressing (HIP) and homogenization, Mater. Sci. Eng. A. 647 (2015) 229–240, https://doi.org/10.1016/j.msea.2015.08.078.
[4] S.G. Ma, Y. Zhang, Effect of Nb addition on the microstructure and properties of AlCoCrFeNi high-entropy alloy, Mater. Sci. Eng. A. 532 (2012) 480–486, https://doi.org/10.1016/j.msea.2011.10.110.
[5] A. Manzoni, H. Daoud, R. Völkl, U. Glatzel, N. Wanderka, Phase separation in equiatomic AlCoCrFeNi high-entropy alloy, Ultramicroscopy 132 (2013) 212–215, https://doi.org/10.1016/j.ultramic.2012.12.015.
[6] T.M. Butler, M.L. Weaver, Oxidation behavior of arc melted AlCoCrFeNi multi-component high-entropy alloys, J. Alloys Compd. 674 (2016) 229–244, https://doi.org/10.1016/j.jallcom.2016.02.257.
[7] J. Zhu, S. Lu, Y. Jin, L. Xu, X. Xu, C. Yin, Y.i. Jia, High-Temperature Oxidation Behaviours of AlCoCrFeNi High-Entropy Alloy at 1073–1273 K, Oxid. Met. 94 (3-4) (2020) 265–281, https://doi.org/10.1007/s11085-020-09991-6.
[8] V. Balaram, Rare earth elements: a review of applications, occurrence, exploration, analysis, recycling, and environmental impact, Geosci. Front. 10 (4) (2019) 1285–1303, https://doi.org/10.1016/j.gsf.2018.12.005.
[9] R. Gawel, Ł. Rogal, J. Dąbek, M. Wójcik-Bania, K. Przybylski, High temperature oxidation behaviour of non-equimolar AlCoCrFeNi high entropy alloys, Vacuum 184 (2021) 109969, https://doi.org/10.1016/j.vacuum.2020.109969.
[10] M. Garg, H.S. Grewal, R.K. Sharma, H.S. Arora, Enhanced Oxidation Resistance of Ultrafine-Grain Microstructure AlCoCrFeNi High Entropy Alloy, ACS Omega 7 (15) (2022) 12589–12600, https://doi.org/10.1021/acsomega.1c0601410.1021/acsomega.1c06014.s001.
[11] X. Zhang, N. Zhang, B. Xing, S. Yin, An Assessment of the High-Temperature Oxidation Resistance of Selected Thermal Sprayed High Entropy Alloy Coatings, J. Therm. Spray Technol. 31 (4) (2022) 1386–1403, https://doi.org/10.1007/s11666-022-01352-w.
[12] Y. Hong, M. Beyramali Kivy, M., Asle Zaeem, Competition between formation of Al2O3 and Cr2O3 in oxidation of Al0.3CoCrCuFeNi high entropy alloy: a first-principles study, Scr. Mater. 168 (2019) 139–143, https://doi.org/10.1016/j.scriptamat.2019.04.041.
[13] Y.u. Liu, G.-P. Zheng, M.o. Li, The effects of short-range chemical and structural ordering related to oxygen interstitials on mechanical properties of CrCoFeNi high-entropy alloys: a first-principles study, J. Alloys Compd. 843 (2020) 156060, https://doi.org/10.1016/j.jallcom.2020.156060.
[14] E. Osei-Agyemang, G. Balasubramanian, Surface oxidation mechanism of a refractory high-entropy alloy, Npj Mater. Degrad. 3 (2019) 1–8, https://doi.org/10.1038/s41529-019-0082-5.
[15] A.J. Samin, A computational investigation of the interstitial oxidation thermodynamics of a Mo-Nb-Ta-W high entropy alloy beyond the dilute regime, J. Appl. Phys. 128 (21) (2020) 215101, https://doi.org/10.1063/5.0028977.
[16] G. Kresse, J. Furthmüller, Efficient iterative schemes for ab initio total-energy calculations using a plane-wave basis set, Phys. Rev. B. 54 (16) (1996) 11169–11186, https://doi.org/10.1103/PhysRevB.54.11169.

[17] G. Kresse, D. Joubert, From ultrasoft pseudopotentials to the projector augmented-wave method, Phys. Rev. B. 59 (3) (1999) 1758–1775, https://doi.org/10.1103/PhysRevB.59.1758.
[18] A. Jain, S.P. Ong, G. Hautier, W. Chen, W.D. Richards, S. Dacek, S. Cholia, D. Gunter, D. Skinner, G. Ceder, K.A. Persson, Commentary: the Materials Project: A materials genome approach to accelerating materials innovation, APL Mater. 1 (1) (2013) 011002, https://doi.org/10.1063/1.4812323.
[19] J.P. Perdew, K. Burke, M. Ernzerhof, Generalized Gradient Approximation Made Simple, Phys. Rev. Lett. 77 (18) (1996) 3865–3868, https://doi.org/10.1103/PhysRevLett.77.3865.
[20] M.C. Payne, M.P. Teter, D.C. Allan, T.A. Arias, J.D. Joannopoulos, Iterative minimization techniques for ab initio total-energy calculations: molecular dynamics and conjugate gradients, Rev. Mod. Phys. 64 (4) (1992) 1045–1097, https://doi.org/10.1103/RevModPhys.64.1045.
[21] H.J. Monkhorst, J.D. Pack, Special points for Brillouin-zone integrations, Phys. Rev. B. 13 (12) (1976) 5188–5192, https://doi.org/10.1103/PhysRevB.13.5188.
[22] A.A. Emery, C. Wolverton, High-throughput DFT calculations of formation energy, stability and oxygen vacancy formation energy of ABO3 perovskites, Sci. Data. 4 (2017), 170153, https://doi.org/10.1038/sdata.2017.153.
[23] A. van de Walle, P. Tiwary, M. de Jong, D.L. Olmsted, M. Asta, A. Dick, D. Shin, Y. Wang, L.-Q. Chen, Z.-K. Liu, Efficient stochastic generation of special quasirandom structures, Calphad. 42 (2013) 13–18, https://doi.org/10.1016/j.calphad.2013.06.006.
[24] L. Wang, S. Seetharaman, Experimental Studies on the Oxidation States of Chromium Oxides in Slag Systems, Metall. Mater. Trans. B. 41 (5) (2010) 946–954, https://doi.org/10.1007/s11663-010-9383-3.
[25] J. Lu, L. Li, H. Zhang, Y. Chen, L. Luo, X. Zhao, F. Guo, P. Xiao, Oxidation behavior of gas-atomized AlCoCrFeNi high-entropy alloy powder at 900–1100 °C, Corros. Sci. 181 (2021) 109257, https://doi.org/10.1016/j.corsci.2021.109257.
[26] Y.a. Wei, Y.u. Fu, Z.-M. Pan, Y.-C. Ma, H.-x. Cheng, Q.-C. Zhao, H. Luo, X.-G. Li, Influencing factors and mechanism of high-temperature oxidation of high-entropy alloys: a review, Int. J. Miner. Metall. Mater. 28 (6) (2021) 915–930, https://doi.org/10.1007/s12613-021-2257-7.
[27] Kinetics of High Temperature Oxidation and Chromia Volatilization for a Binary Ni–Cr Alloy | SpringerLink, (n.d.). https://link.springer.com/article/10.1007/s11085-005-6562-8 (accessed November 18, 2021).